Optical zooming interferometer for subnanometer positioning using an optical frequency comb

Mariko Kajima* and Kaoru Minoshima

National Institute of Advanced Industrial Science and Technology (AIST), 1-1-1 Umezono, Tsukuba 305-8563, Ibaraki, Japan

*Corresponding author: m.kajima@aist.go.jp

Received 12 May 2010; revised 9 August 2010; accepted 26 September 2010; posted 29 September 2010 (Doc. ID 128288); published 15 October 2010

A high-precision positioning stage based on an optical zooming interferometer is proposed. Two external-cavity diode lasers, stabilized to a femtosecond optical frequency comb, are used as optical sources. The zooming principle is demonstrated, and the positioning resolution of 0.2 nm is achieved. The positioning accuracy was partly evaluated. © 2010 Optical Society of America

OCIS codes: 120.3180, 120.3930.

1. Introduction

The demand for high resolution and high accuracy in absolute measurements of displacement is increasing. High-precision measurement systems of displacement lead to the development of high-precision instruments for displacement or position measurement. For the purpose of calibration of those displacement- or position-measuring instruments, a SI-traceable positioning stage with a subnanometer resolution and subnanometer accuracy is necessary. The laser interferometer is a suitable system for the calibration of precise displacement-measuring instruments because it is safe, simple, and is directly traceable to the metric system. However, conventional laser interferometers, whether homodyne or heterodyne, have cyclic errors of several nanometers [1–4]. Much effort has been made to remove cyclic errors in laser interferometers [5,6]. Certain laser-frequency-based methods for displacement measurement were proposed in [7,8]. Frequency-based methods do not lead to cyclic errors, in principle, and have direct traceability to frequency. In those methods, a widely frequency-tunable light source is necessary to realize long movable range displacement measurements. For nanometrological calibration, an x-ray interferometer system [9], an atomic force microscope with laser interferometers [10], and a high-precision scanning tunneling microscope [11] were developed. Although these systems have high resolutions that reach subnanometer levels, they have some practical problems, such as the large size of the system and they could cause safety issues.

An optical zooming interferometer was proposed in order to achieve a positioning stage with high resolution and high accuracy [12]. The zooming interferometer has two optical sources and two movable stages. Two interferometers, with different optical sources, were combined in one zooming interferometer. When one of the movable stages (course stage) displaces, the phases in two interferometers shift. The phase shifts in the interferometers are slightly different. The other movable stage (fine stage) in the zooming interferometer is displaced so that the differences in phase shifts are compensated to be zero. Thus, the displacement of the course stage is reduced to the fine stage. The zooming interferometer plays the role of Vernier, and a high-resolution movable stage can be realized. The ratio of the magnitude of displacement of the course stage to that of the fine stage is called the "zooming ratio." When the displacement of the course stage was measured by a traceable length measurement system, the reduced displacement of the fine stage can be determined traceably. The accurate determination of the zooming ratio is

0003-6935/10/305844-07$15.00/0

necessary for accurate positioning of the latter movable stage. The optical zooming interferometer in Ref. [12] used refractive index dispersion to create the scaling-down mechanism. An optical zooming method that used optical sources, which had slightly different wavelengths, was proposed in Ref. [13]. It used two wavelengths of a Zeeman-stabilized He–Ne laser as optical sources. The zooming ratio was determined based on the ratio of the difference in wavelengths to one of the wavelengths in a Zeeman-stabilized He–Ne laser. Since the difference in wavelengths of a Zeemen-stabilized He–Ne laser was very small, the zooming ratio was very small and a high resolution was achieved. However, the extremely small zooming ratio resulted in a limited movable range.

To expand the movable range of the positioning stage, we proposed a new type of zooming interferometer [14]. In that system, the zooming ratio was determined by the ratio of the wavelength of stabilized He–Ne laser and the synthetic wavelength of two external-cavity diode lasers (ECLDs). By using two independent tunable lasers, the synthetic wavelength was variable and the zooming ratio was tunable to the suitable value. Consequently, the limit of the movable range of the positioning stage becomes long. The synthetic wavelength of ECLDs was stabilized by using a femtosecond optical comb (fs-comb) so that high-accuracy and frequency-traceable measurements could be realized. However, the optical system was big and complex due to the use of three lasers, and the stability was not reached in the subnanometer region. In addition, the accuracy of the zooming ratio was not evaluated enough because of the use of low-resolution displacement sensors for the measurement of displacements of movable stages.

In this study, we developed a zooming interferometer whose optical sources were two ECLDs with slightly different wavelengths. The zooming ratio was determined based on the ratio of the difference of wavelengths of ECLDs to the wavelength of one of the ECLDs. Because the center wavelengths of the ECLDs were stabilized using a fs-comb, a stable and tunable zooming ratio could be obtained. The zooming ratio was tuned to the suitable value for displacement- or position-measuring instruments, approximately 1.7×10^{-3}. The optical system became simple and small by using only two optical sources, and the high-resolution displacement sensors were used for evaluation of the zooming ratio in this study.

In this paper, we demonstrate the displacement-reduction principle of the developed zooming interferometer. The stability, linearity, and resolution of positioning were determined for the first step of estimation of total uncertainty of the positioning system.

2. Optical Zooming Interferometer

An optical zooming interferometer consists of two interferometers with optical sources of slightly different wavelengths. Figure 1 shows the schematic diagram of the proposed zooming interferometer. The black lines denote the optical path of the first interferometer. The wavelength of the first interferometer's optical source is λ_1. A movable reflector, R1, and a fixed reflector, R3, are set in the optical path of the first interferometer. The dashed lines denote the optical path of the second interferometer. The wavelength of the second interferometer's optical source is λ_2. The two movable reflectors, R1 and R2, are set in the optical path of the second interferometer. R1 is common to both interferometers. The photodetectors, PD1 and PD2, detect the light intensity of wavelengths λ_1 and λ_2, respectively. The lock-in amplifier compares the phase changes in the first and the second interferometers. The difference between the phase changes is fed back to the displacement of R2 through a proportional-integral-derivative (PID) controller so that the phase-change difference is always zero.

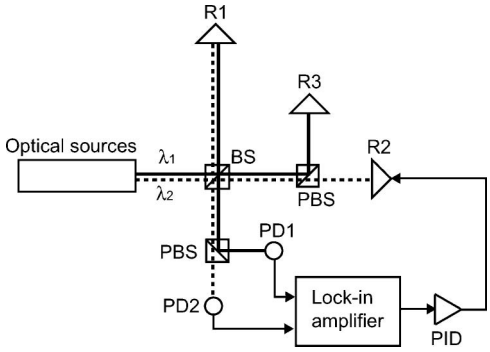

Fig. 1. Schematic diagram of the zooming interferometer. Solid line, optical path of the first interferometer with wavelength λ_1; dashed line, optical path of the second interferometer with wavelength λ_2.

When R1 and R2 are displaced by a distance of X_1 and X_2, respectively, the phase changes of the two interferometers are determined by

$$\delta\phi_1 = 2\pi n_1 \frac{X_1}{\lambda_1}, \tag{1}$$

$$\delta\phi_2 = 2\pi n_2 \frac{(X_1 - X_2)}{\lambda_2}, \tag{2}$$

where n_1 and n_2 are the refractive indices of air at wavelengths λ_1 and λ_2, respectively. When R1 moves by a distance X_1, the displacement of R2 is controlled so that the phase changes of the two interferometers are the same:

$$\Delta\phi = \delta\phi_1 - \delta\phi_2 = 2\pi\left(\frac{n_1 X_1}{\lambda_1} - \frac{n_2(X_1 - X_2)}{\lambda_2}\right) = 0. \tag{3}$$

As a consequence, the relation between the displacement of R1 and that of R2 is expressed as

$$X_2 = \frac{\lambda_1 - \frac{n_1}{n_2}\lambda_2}{\lambda_1} \cdot X_1. \tag{4}$$

When the wavelengths, λ_1 and λ_2, are almost the same, the refractive indices are almost the same, i.e., $n_1 \approx n_2$; then

$$X_2 = \frac{\lambda_1 - \lambda_2}{\lambda_1} \cdot X_1. \tag{5}$$

The magnitude of the displacement X_2 is proportionally smaller, compared to X_1. The ratio of displacement X_2 to X_1 is called the zooming ratio, K:

$$K = \frac{\lambda_1 - \lambda_2}{\lambda_1}. \tag{6}$$

The zooming ratio is determined only by the values of λ_1 and $\lambda_1 - \lambda_2$. When wavelengths λ_1 and λ_2 are nearly equal, the zooming ratio, K, is small. This small zooming ratio allows the movement of R2 to be controlled finely by coarse movement of R1. A high-resolution control of the displacement of R2 is realized by this principle. This control mechanism of the displacement of R2 is the zooming control. When the displacement of R1 is measured by a traceable laser interferometer, this positioning system can be applied to traceable displacement measurement. The cyclic error in the laser interferometer, which was used for the measurement of displacement of R1, can be reduced by the zooming ratio in the displacement of R2. For accurate determination of the displacement of R2 by using a zooming interferometer, accurate determination of the zooming ratio is essential. To determine the zooming ratio accurately, the wavelengths of the optical sources and the wavelength difference between the optical sources must be stabilized. Although the error in the laser interferometer, which is used for displacement measurement of R1, is reduced by the zooming system, the errors that are caused by the zooming interferometer itself cannot be reduced. The careful treatment of mixing of polarization in the zooming interferometer and stabilization of the environment are necessary to reduce errors in the zooming interferometer.

3. Experimental Setup

We used two ECLDs as optical sources for the zooming interferometer. The center frequencies of the two ECLDs were at approximately 781 and 780 nm. For the purpose of obtaining an accurate and stable zooming ratio, these two ECLDs were stabilized to two modes in a fs-comb with a repetition frequency of 48 MHz, the central wavelength of 780 nm, and the FWHM of 7.5 nm. Figure 2 shows the stabilization system of the optical sources. The detailed scheme of stabilization of the optical sources was explained in Ref. [14]. The beat frequency between ECLD1 and one of the modes in the fs-comb was controlled to 1.25 MHz so that the center wavelength of ECLD1 was stabilized to the fs-comb. ECLD2 was stabilized to a different mode in the same fs-comb. The fs-comb that was used in this experiment did not have the direct control mechanism of the repetition rate nor the offset frequency, i.e., free-run comb. In order to improve the frequency stability of the fs-comb, we controlled the ambient temperature of the laser cavity of the fs-comb to fluctuate less than 5 mK in 1 h.

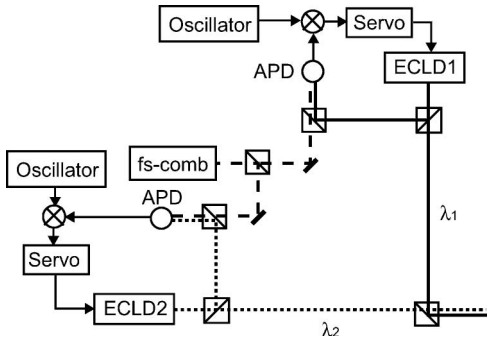

Fig. 2. Stabilization system of two ECLDs by using a fs optical comb.

The center wavelength of each ECLD, which was one factor of the zooming ratio, was measured by a wavemeter with an accuracy of 0.03 pm. The standard deviation of the wavelength for 500 s of each ECLD, which was stabilized by the ambient-temperature-stabilized fs-comb, was 0.03 pm, which was the same level as the precision of the wavemeter. The relative stability of the center wavelength of each ECLD compared to the center wavelength was 4×10^{-8}. The wavelength difference between ECLD1 and ECLD2, which was another factor of the zooming ratio, was also stabilized by using the fs-comb. The frequency difference between ECLD1 and ECLD2, Δf, was determined as

$$\Delta f = f_2 - f_1 = m \cdot f_{\mathrm{rep}} + f_{1\mathrm{beat}} - f_{2\mathrm{beat}}, \tag{7}$$

where f_1 and f_2 were the center frequencies of ECLD1 and ECLD2, f_{rep} was the repetition frequency of the fs-comb, m was the number of the comb's modes that existed between f_1 and f_2, and $f_{1\mathrm{beat}}$ and $f_{2\mathrm{beat}}$ were the beat frequencies between the ECLDs and the comb's modes, to which the ECLDs were stabilized. The frequency difference, Δf, was approximately 0.5 THz, and f_{rep} was 48 MHz. Therefore, m was approximately 10,000. $f_{1\mathrm{beat}}$ and $f_{2\mathrm{beat}}$ were 1.25 MHz. The stability of Δf, $\delta\Delta f$, was calculated as

$$\delta\Delta f^2 = m \cdot \delta f_{\mathrm{rep}}{}^2 + \delta f_{1\mathrm{beat}}{}^2 + \delta f_{2\mathrm{beat}}{}^2, \tag{8}$$

where δf_{rep} was the standard deviation of f_{rep}, and $\delta f_{1\mathrm{beat}}$ and $\delta f_{2\mathrm{beat}}$ were the standard deviation of $f_{1\mathrm{beat}}$ and $f_{2\mathrm{beat}}$. The repetition frequency was measured by a frequency counter with the gate time of 1 s. The standard deviation of the repetition frequency, δf_{rep}, in the measurement time of 100 s was 0.05 Hz. $\delta f_{1\mathrm{beat}}$ and $\delta f_{2\mathrm{beat}}$ were calculated from the signals of frequency differences from the frequency reference of 1.25 MHz. $\delta f_{1\mathrm{beat}}$ and $\delta f_{2\mathrm{beat}}$ were 4.9 and 5.4 kHz in the measurement time of 100 s. Thus, the stability of

the beat frequency of ECLD1 and ECLD2 was

$$\delta\Delta f = \sqrt{10000 \times 0.05^2 + (4.9 \times 10^3)^2 + (5.4 \times 10^3)^2} = 7.3\,\text{kHz}. \quad (9)$$

It was equivalent to the stability of 1.4×10^{-8} compared to the frequency difference, Δf, of 0.5 THz. Consequently, the relative stability of the zooming ratio, $\delta K/K$, which was calculated from the stability of the center wavelength of an ECLD and the stability of the frequency difference between ECLD1 and ECLD2, reached 4×10^{-8} by using the ECLDs that were stabilized to a fs-comb.

The difference in optical path lengths of the interferometer arms, i.e., the dead path, was less than 1 mm in the improved optical setup of this experiment. The long-term drift of the wavelength of each ECLD, which was calculated by fitting the slope of the wavelength variation to time, was 1.6×10^{-7} nm for a measurement time of 500 s. Therefore, the calculated dead path fluctuation, which was caused by the wavelength drift, was reduced to the subpicometer range, and therefore its effect was negligible.

The experimental setup is shown in Fig. 3. The optical path of the first interferometer in the zooming interferometer with an optical source of wavelength λ_1 equal to 781 nm, is indicated by black lines. The optical path of the second interferometer with an optical source of wavelength λ_2 equal to 780 nm is indicated by dashed lines. In the first interferometer, one of the laser beams that was divided by a beam splitter (BS) passed the fixed optical path, and the other laser beam was frequency-shifted by an acousto-optic modulator (AOM) and reflected by the movable reflector R1. In the second interferometer, one of the laser beams, which was divided by a BS, was reflected by a movable reflector R2, and the other laser beam was frequency-shifted by the AOM, which was the same AOM as in the first interferometer, and reflected by the movable reflector R1. The AOM was used for the purpose of detecting the phase change of the two interferometers by using a lock-in amplifier. The modulation frequency of the AOM was 79.9 MHz. Two polarizers, P1 and P3, were used to separate the two light sources along different optical paths. Two additional polarizers, P2 and P4, were set in front of the detectors so that the detectors only detected the light sources of λ_1 and λ_2, respectively.

A stepper motor stage with a resolution of 1 nm was used as a coarse positioning stage of R1. The stepper motor stage was made of low-thermal-expansion cast iron, whose thermal expansion coefficient was 2.5×10^{-6}. A piezoelectric actuator (PZT) stage without built-in position control was used as a fine positioning stage of R2. The position of R2 was controlled by the zooming mechanism following the displacement of R1. The phase changes in the first and second interferometer were compared by means of a lock-in amplifier. The phase-change difference, $\Delta\phi$, was converted to a voltage in the lock-in amplifier, and the voltage was fed back to the PZT stage by a PID controller. The displacement of R2 was controlled by the feedback voltage from the PID controller during the zooming control. The optical system of the zooming interferometer was fixed on a base plate with low thermal expansion to eliminate the thermal expansion of the optical path. The optical system was covered by an insulation box.

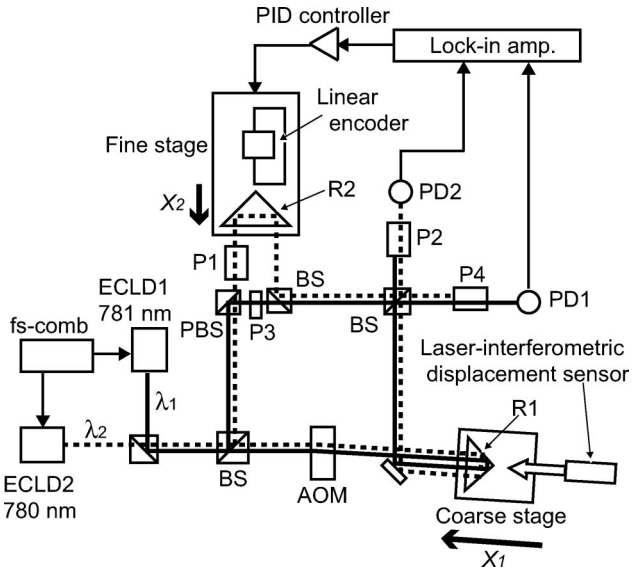

Fig. 3. Experimental setup of the zooming interferometer. Solid line, optical path of the first interferometer with wavelength λ_1; dashed line, optical path of the second interferometer with wavelength λ_2; R1, R2, corner reflectors; PBS, polarizing beam splitter; PD, photodetector.

4. Experiments and Results

To evaluate the positioning ability of the fine stage controlled by the zooming system, we investigated the stability, linearity, and resolution of positioning. These were important parts of sources of estimating uncertainty of positioning. For the purpose of evaluation of the zooming control, a laser-interferometric displacement sensor (1.2 nm resolution, Agilent Technologies) and a linear encoder (35 pm resolution, BS78, Sony Manufacturing Systems) were used to measure the displacement of R1 and R2, respectively. The reflector of the laser-interferometric displacement sensor was fixed on the same aluminum base plate as R1. The scale of the linear encoder was attached to the same aluminum base plate as R2, and the reading head of the encoder was fixed on the base plate of the zooming interferometer. The displacement sensor and the linear encoder were used only for monitoring and evaluating the displacement of R1 and R2, and not for zooming control. The wavelengths of the optical sources were measured with a wavemeter to calculate the theoretical zooming ratio by substituting wavelengths in Eq. (6).

The cosine errors of the stage settings were compensated in the experiments in this paper by measuring the stage displacements both by interferometers that configured the zooming interferometer and the

displacement sensors. For compensation of the setting error of the coarse stage, the displacement of R1 was measured by one of the interferometers in the zooming interferometer with the optical source of ECLD1 and by the laser-interferometric displacement sensor at the same time. The ratio of the measured values was considered as the setting error. The measured values by the laser-interferometric displacement sensor in the experiments in this paper were compensated by multiplying the ratio of the measured values mentioned above. The setting error of the fine stage was compensated by multiplying the ratio of the measured values of the displacement of R2 by using the interferometer with the optical source of ECLD2 and by using the linear encoder to the measured values by the linear encoder in the experiments in this paper.

A. Positioning Stability

The positioning stability was investigated by measuring the position of R2 with a linear encoder. The positioning stability was the indicative factor of the fluctuations in the zooming interferometer. The position of R2 was controlled by the zooming control while the position of R1 was fixed. The gray line in Fig. 4 shows the position of R2 measured by the linear encoder. The sampling rate was 100 Hz. The drift in the position of R2, which was calculated as the gradient of linear fitting to the position of R2, was 0.04 nm at 100 s. The position of R2 shows a short-cycle fluctuation, where the cycle was less than 0.2 s, and a long-period fluctuation, where the cycle was about 25 s. The standard deviation of the short-cycle fluctuation was 0.6 nm. The short-cycle fluctuation was thought to be electrical and seismic noise. Improving the electrical system and the vibration control could reduce the fluctuation further. The black points in Fig. 4 show the 100-point moving average of the position data of R2. An apparent 25 s cycle fluctuation is shown. The amplitude of this long-period fluctuation varied with time. The typical peak-to-peak amplitude was 0.6 nm. The cause of this long-period fluctuation was thought to be the fluctuation in temperature and air pressure.

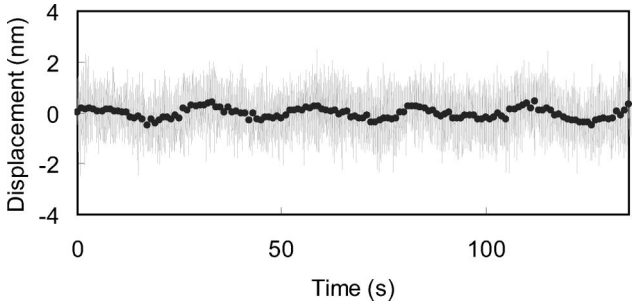

Fig. 4. Positioning stability: gray line, the position of R2 while R1 was fixed in the zooming control; black points, 100 time-averaged positioning fluctuations.

B. Linearity of Positioning

For the purpose of verifying the zooming principle, we measured the fine displacement of R2, which was caused by the coarse displacement of R1 during the zooming control. In this experiment, R1 was displaced at a constant speed, 1 μm/s, by the stepper motor stage. The displacement of R1 was measured by a laser-interferometric displacement sensor, and the displacement of R2 was measured by a linear encoder. Figure 5(a) shows the displacement of R2 compared to the displacement of R1. It shows that the displacement of R2 was inversely proportional to the displacement of R1, which is the zooming principle. R1 was displaced by 500 μm, and R2 was displaced by about 865 nm. Based on linear fitting to the slope of Fig. 5(a), the measured zooming ratio was determined to be $K = 1.718 \times 10^{-3}$. The wavelengths of ECLD1 and ECLD2 at the time of this experiment were 781.130 and 779.782 nm, respectively. The theoretical zooming ratio, which was calculated based on Eq. (6) by using the measured wavelengths was 1.726×10^{-3}. There is a discrepancy of 8×10^{-6} between the measured and the theoretical zooming ratio. This discrepancy was equivalent to a displacement error of about 4 nm in the total 865 nm displacement of R2. The cause of the discrepancy between the measured and the theoretical zooming ratio is discussed in Section 5.

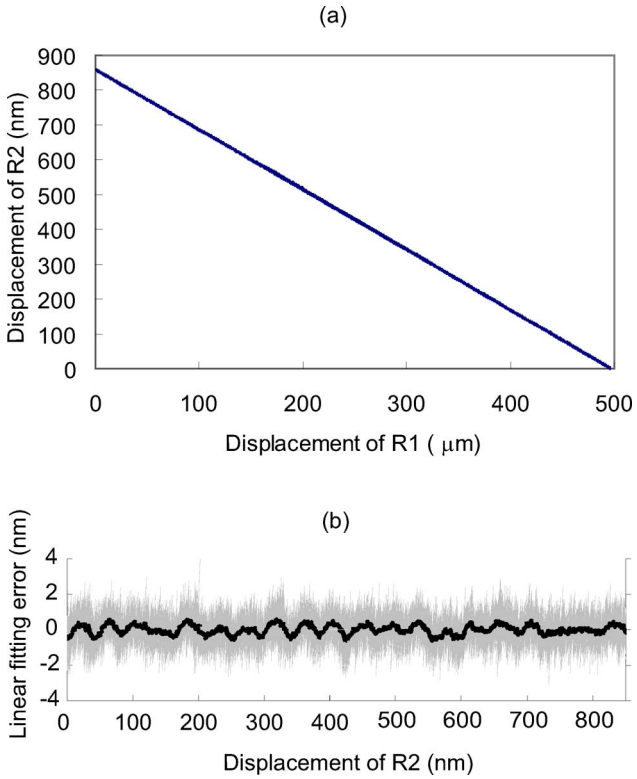

Fig. 5. (a) Linearity of displacement. Displacement of R2 compared to the displacement of R1 was proportional. (b) Linear fitting error. The horizontal axis is the displacement of R2. Gray line, nonlinear residuals; black points, 100 time moving average of nonlinear residuals.

The residual error of the linear fitting to the slope of Fig. 5(a) is shown in Fig. 5(b). In this graph, the horizontal axis shows the displacement of R2, and the vertical axis shows the nonlinear residuals. The gray line shows the residual error of the linear fitting. The standard deviation of the nonlinear residuals was 0.7 nm, which included electrical noise and seismic noise. The black points show the 100-point moving average of the residuals. In the moving average, high-frequency noise, such as electrical and seismic noise, was averaged out and disappeared. The moving average shows a periodic curve of the period of about 40 nm for the displacement of R2. The period of this curve was equivalent to a 25 s cycle. This cycle was the same as the time cycle of the long-period fluctuation that appeared in the stability test mentioned in Subsection 4.A, and it did not conform to the cycle of the optical cyclic error of the laser-interferometric displacement sensor used for the measurement of displacement of R1. The cause of this periodic curve was thought to be the fluctuation in temperature and air pressure, which was the same cause as in the stability test. It showed that the cyclic error of the laser-interferometric displacement sensor was eliminated in accordance with the zooming principle and that electrical and environmental fluctuation noise in the zooming interferometer remained as the errors in the linearity of the positioning.

C. Positioning Resolution

We did the step-by-step displacement test to determine the positioning resolution of R2 by the zooming control. In this experiment, R1 was displaced by 600 nm in 2 s, stopped for 5 s, then repeated the movement. The displacement of R2 was controlled by the zooming control following the displacement of R1. Figure 6 shows the step-by-step displacement of R2, which was measured by the linear encoder. The average of the displacement steps was 1.1 nm. The standard deviation of the displacement of R2 for 1 s while R2 was stopped was 0.2 nm, which was the resolution of the positioning of R2. This resolution was not determined based on the limit of the zooming principle but based on the electrical and seismic noise in the experimental setup with the linear encoder and the control system.

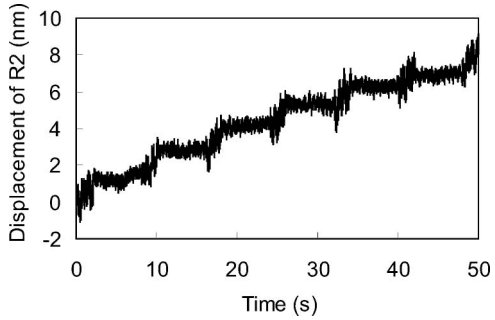

Fig. 6. Step-by-step displacement of R2. R1 was displaced by 600 nm in a staircase pattern. The displacement step of R2 was reduced to 1.1 nm. The resolution of the system was determined to be 0.2 nm.

5. Discussion

In the above experiments, a discrepancy between the measured zooming ratio and the theoretical zooming ratio was observed. To determine the cause of the discrepancy, a series of measurements of the zooming ratio were conducted. In this experiment, R1 was displaced ten round trips of 500 μm in a series. R2 was displaced by the zooming control along ten round trips of about 850 nm following the displacement of R1. The measured zooming ratio was obtained for each one-way displacement from the slope of the linear fitting of the measured displacement of R2 to the applied displacement of R1, as mentioned in Subsection 4.B. We obtained 20 measured zooming ratios by ten round-trip displacements. Figure 7 shows the result of the repeated measurements of the zooming ratio. The black circles show the measured zooming ratios in forward movement of R2, and the white circles show the measured zooming ratios in backward movement of R2. The difference between the measured and the theoretical zooming ratios was 4×10^{-7}, which was equivalent to the discrepancy of 0.2 nm in the total displacement of 850 nm of R2. The repeatability error, which was calculated as the standard deviation of 20 measured zooming ratios divided by the square root of the repeat count, 20, was 3.8×10^{-6}, shown as error bars in the graph. The average of the measured zooming ratio and the theoretical zooming ratio agreed to within the repeatability error. Since the wavelength fluctuation was sufficiently small, the remaining discrepancy of the zooming ratio was thought to be caused by some systematic errors in the zooming interferometer itself. This error was not eliminated by the zooming principle, and it was directly added to the positioning accuracy of the fine stage. In this experiment, the largest cause of variation of the zooming ratio was thought to be temperature change of the aluminum base plate on which R2 and the scale of the encoder were fixed. It is clearly shown in Fig. 7 that the zooming ratios in forward movements of R2, indicated by black circles, were smaller than the average of the 20 zooming ratios. On the other hand, the

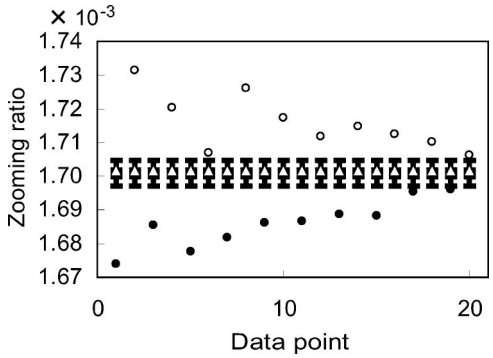

Fig. 7. Twenty repeated measurements of the zooming ratio. Filled circles, zooming ratio in the forward movement; open circles, zooming ratio in the backward movement; triangles, averaged measured zooming ratio; squares, theoretical zooming ratio calculated based on measured wavelengths of optical sources.

zooming ratios in backward movements of R2, indicated by white circles, were larger than the average. The measured zooming ratios varied significantly the first several times and steadily converged to a value—the average of the 20 measured zooming ratios. Considering these characteristic patterns, the unidirectional thermal expansion of the base plate caused a discrepancy between the displacement of R2 and the measured value of the linear encoder. The total temperature change of the base plate was 0.2 K, and the separation between R2 and the scale was 8 cm. The total thermal expansion of the separation was estimated as 380 nm, which was the same order with the total discrepancy of the zooming ratio. This value was larger than the stability mentioned in Subsection 4.A, since the ten round-trip test took a longer time and the stepper motor caused heat by movement. The error in the zooming ratio would be reduced by averaging repeated measurements or by starting measurements after enough time has passed and the stage has reached thermal equilibrium. To avoid thermal expansion of the base plate, it would be better to put the laser-interferometric displacement sensor to the identical axis orientation with the arm of the zooming interferometer. Adding temperature control for the aluminum base plate to which R2 and the linear encoder were attached or replacing the aluminum base plate by low-thermal-expansion material are also effective countermeasures.

6. Conclusion

An improved setup for the optical zooming interferometer with the two ECLDs that were stabilized to an ambient-temperature-stabilized fs-comb was developed, and parts of the positioning ability, stability, linearity, and resolution of the zooming system were examined. By the zooming principle, the linear reduction of the displacement of R1 was demonstrated, and a high positioning resolution, 0.2 nm, was realized, even though it included noises in the zooming interferometer. The positioning stability and nonlinearity were improved by stabilizing the optical system. There were residual errors in the zooming interferometer. The positioning stability, 0.6 nm, showed the electrical, seismic, and environmental fluctuation. The discrepancy between the measured and the theoretical zooming ratio and variation of the measured zooming ratio appeared, and the positioning error caused by the error of the zooming ratio was 0.2 nm even after an average of 20 measurements. The error in the zooming ratio would be reduced by the treatment of environmental fluctuation and use of low-thermal expansion materials for base plates.

In this experiment, wavelengths of the lasers and environmental sensors were not yet calibrated. To apply this system to a traceable calibration system for displacement sensors, the additional estimation of total uncertainty including calibration uncertainties of wavelengths, environmental sensors, and cosine and Abbe errors is indispensable. Although the displacement range was 850 nm in this experiment, it could easily be expanded to 16 μm, which is the movable range of the PZT stage, only by replacing the control circuit in the system using a suitable PZT amplifier; thus, the zooming principle would not limit the movable range.

This research was partially supported by the New Energy and Industrial Technology Development Organization. We are grateful to Hirokazu Matsumoto of the University of Tokyo for his contributions during the early stages of this work.

References

1. C. M. Wu and R. D. Deslattes, "Analytical modeling of the periodic nonlinearity in heterodyne interferometry," Appl. Opt. **37**, 6696–6700 (1998).
2. N. Bobroff, "Recent advances in displacement measuring interferometry," Meas. Sci. Technol. **4**, 907–926 (1993).
3. L. Chassagne, S. Topcu, Y. Alayli, and P. Juncar, "Highly accurate positioning control method for piezoelectric actuators based on phase-shifting optoelectronics," Meas. Sci. Technol. **16**, 1771–1777 (2005).
4. C. M. Wu and C. S. Su, "Nonlinearity in measurements of length by optical interferometry," Meas. Sci. Technol. **7**, 62–68 (1996).
5. T. Keem, S. Gonda, I. Misumi, Q. Huang, and T. Kurosawa, "Simple, real-time method for removing the cyclic error of homodyne interferometer with a quadrature detector system," Appl. Opt. **44**, 3492–3498 (2005).
6. J. Lawall and E. Kessler, "Michelson interferometry with 10 pm accuracy," Rev. Sci. Instrum. **71**, 2669–2676 (2000).
7. L. Howard, J. Stone, and J. Fu, "Real-time displacement measurements with a Fabry–Perot cavity and a diode laser," Precis. Eng. **25**, 321–335 (2001).
8. T. R. Schibli, K. Minoshima, Y. Bitou, F. L. Hong, H. Inaba, A. Onae, and H. Matsumoto, "Displacement metrology with sub-pm resolution in air based on a fs-comb wavelength systhesizer," Opt. Express **14**, 5984–5993 (2006).
9. G. Basile, P. Becker, A. Bergamin, G. Cavagnero, A. Franks, K. Jackson, U. Kuetgens, G. Mana, E. W. Palmer, C. J. Robbie, M. Stedman, J. Stümpel, A. Yacoot, and G. Zosi, "Combined optical and x-ray interferometry for high-precision dimensional metrology," Proc. R. Soc. London Ser. A **456**, 701–729 (2000).
10. S. Gonda, T. Doi, T. Kurosawa, and Y. Tanimura, "Real-time, interferometrically measuring atomic force microscope for direct calibration on standards," Rev. Sci. Instrum. **70**, 3362–3368 (1999).
11. M. Aketagawa, H. Honda, M. Ishige, and C. Patamaporn, "Two-dimensional encoder with picometer resolution using lattice spacing on regular crystalline surface as standard," Meas. Sci. Technol. **18**, 342–349 (2007).
12. H. Matsumoto and K. Minoshima, "High-accuracy ultrastable moving stage using a novel self-zooming optical scale," Opt. Commun. **132**, 417–420 (1996).
13. Y. Zhao, X. H. Cheng, and D. C. Li, "Dual-wavelength parallel interferometer with superhigh resolution," Opt. Lett. **27**, 503–505 (2002).
14. M. Kajima and H. Matsumoto, "Picometer positioning system based on a zooming interferometer using a femtosecond optical comb," Opt. Express **16**, 1497–1506 (2008).